HOSTED BY

ELSEVIER

Available online at www.sciencedirect.com

ScienceDirect

Soils and Foundations xxx (xxxx) xxx

SOILS AND FOUNDATIONS

www.elsevier.com/locate/sandf

Technical Paper

Deformation and cyclic resistance of sand in large-strain undrained torsional shear tests with initial static shear stress

Muhammad Umar [a], Gabriele Chiaro [b,*], Takashi Kiyota [a], Nazish Ullah [c]

[a] *Institute of Industrial Science, The University of Tokyo, Japan*
[b] *Department of Civil and Natural Resources Engineering, University of Canterbury, New Zealand*
[c] *Civil Engineering Department, The University of Tokyo, Japan*

Received 1 October 2020; received in revised form 13 February 2021; accepted 27 February 2021

Abstract

This paper presents the findings from an experimental study focusing on the undrained cyclic behavior of sand in the presence of initial static shear stress. A series of undrained cyclic torsional shear tests was performed on saturated air-pluviated Toyoura sand specimens up to single amplitude shear strain (γ_{SA}) exceeding 50%. Two types of cyclic loading conditions, namely, stress reversal (SR) and stress non-reversal (SNR), were employed by changing the amplitude of the combined initial static shear and cyclic shear stresses. The tests covered a broad range of initial states in terms of relative density ($Dr = 20$–74%) and the initial static shear stress ratio ($\alpha = 0$–0.30). The following five distinct modes of deformation were identified from the tests based on the density state, the transient undrained peak shear stress, and the combined cyclic and static shear stresses: 1) static liquefaction, 2) cyclic liquefaction, 3) cyclic mobility, 4) shear deformation failure, and 5) limited deformation. Of these, cyclic liquefaction and static liquefaction are the most critical. They occur in very loose sand ($D_r \leq 24\%$) under SR and SNR, respectively, and are characterized by abrupt flow-type shear deformation. Cyclic mobility occurs under SR in loose to dense sand with $D_r \geq 24\%$. Contrarily, shear deformation failure typically occurs under SNR in sand with $24 < D_r < 65\%$, and limited deformation may take place in dense sand with $D_r \geq 65\%$. In this paper, a stress-void ratio-based predictive method is proposed to identify the likely mode of deformation/failure in sand under undrained shear loading with static shear. Furthermore, the cyclic resistance is evaluated at three different levels of γ_{SA} (i.e., small, $\gamma_{SA} = 3\%$; moderate, $\gamma_{SA} = 7.5\%$; and large, $\gamma_{SA} = 20\%$). The results show that, independent of the density state, the cyclic resistance continuously decreases with an increase in α at the small γ_{SA} level, while it first decreases and then increases for both loose and dense sand at the moderate and large γ_{SA} levels.

Keywords: Initial static shear; Liquefaction; Large shear strain; Torsional shear; Cyclic resistance

1. Introduction

Under sloping ground conditions, the stress state acting on a soil element is recognized as being different from that under level ground conditions, due to the presence of gravitationally induced static shear stress. Lee and Seed (1967), Lee and Albaisa (1974), and Seed (1981) carried out pioneering studies on the influence of static shear stress on the cyclic resistance of sand using anisotropically consolidated triaxial specimens. They reported that the presence of static shear increases the cyclic resistance. Vaid and Chern (1983, 1985) and Hyodo et al. (1991) conducted triaxial tests and found that the cyclic resistance can increase or decrease due to the presence of static shear

Peer review under responsibility of The Japanese Geotechnical Society.
* Corresponding author.
E-mail addresses: umar@iis.u-tokyo.ac.jp (M. Umar), gabriele.chiaro@canterbury.ac.nz (G. Chiaro), kiyota@iis.u-tokyo.ac.jp (T. Kiyota), nazish@iis.u-tokyo.ac.jp (N. Ullah).

https://doi.org/10.1016/j.sandf.2021.02.008
0038-0806/

stress, depending on the density state, the magnitude of static shear, and the definition of liquefaction. More recently, Yang and Sze (2011) showed that the cyclic resistance of sand always increases with an increase in relative density, with or without static shear.

It is well accepted that simple shear tests can reproduce the conditions of field stress that are expected during earthquakes more accurately than triaxial tests. Yoshimi and Oh-oka (1975), Vaid and Finn (1979), and Tatsuoka et al. (1982) conducted ring shear, direct shear, and torsional shear tests, respectively, applying static shear stress on sandy soils. They reported conflicting conclusions to those by Lee and Seed (1967) based on triaxial tests. They found that the cyclic resistance can either increase or decrease due to the presence of static shear, depending on the relative density and the combination of static and cyclic stresses. Vaid et al. (2001) and Sivathayalan and Ha (2011) conducted simple direct shear tests and concluded that the presence of static shear increases the cyclic resistance of dense sand and decreases it for loose sand. Chiaro et al. (2012) and Umar et al. (2016a) highlighted the importance of the strain level on the evaluation of the cyclic resistance of sand subjected to static shear stress. They conducted large-strain simple shear tests (double amplitude shear strain, γ_{DA} up to 100%) on loose sand with static shear by employing the modified torsional shear device developed by Kiyota et al. (2008). They found that the resistance to the accumulation of small strain, as a result of cyclic loading, always decreases, but that the resistance to the accumulation of large strain first decreases and then increases. The identification and classification of deformation modes in the presence of static shear are of paramount importance for properly assessing the extent of the damage to liquefied sloping grounds. Based on the difference in the effective stress paths and stress–strain relationships in the triaxial tests, Hyodo et al. (1991) categorized the loading types into stress reversal (SR) and stress non-reversal (SNR). They found that sand failure could be associated with liquefaction in the SR case. In contrast, failure resulted from the accumulation of residual shear deformation without liquefaction in the SNR case. Yang and Sze (2011) and Chiaro et al. (2012) reported three different deformation modes related to initial static shear: flow-type failure, cyclic mobility, and accumulated plastic shear strain. Yang and Pan (2017) reported that very loose sand developed flow-type failure and was unaffected by stress reversal loading conditions. They also stressed the importance of the shearing mode in triaxial tests, i.e., the application of static shear in triaxial compression or extension influences the mode of deformation in the sand.

Presently, for the mode of cyclic mobility and accumulated plastic shear strain, the general approach is to define failure based on the development of specified single amplitude shear strain (Chiaro et al., 2012). In the case of flow failure, such a criterion is inapplicable due to the small level of shear strain that usually develops before failure. Therefore, there is a need to establish a unique and robust predictive method for assessing the likely mode of the deformation of sand due to the presence of static shear stress. Considering the above background, the aim of the present study is to provide new insights into the deformation modes and cyclic strength of sand, from very loose to dense states (as defined in Table 1), up to the large shear strain level of 20%. Furthermore, a predictive method is proposed for different density states based on the combined cyclic and static shear stresses, the transient undrained peak shear stress, and the density state. Correction factor K_α, defined as the ratio of the cyclic resistance of soils with static shear to that without static shear (Seed, 1983), is used to quantify the effects of initial static shear on the cyclic resistance of sand, from small to large shear strain levels, for different density states.

2. Test apparatus, material, and procedure

Laboratory tests were carried out using the fully automated torsional apparatus developed at the Institute of Industrial Science, University of Tokyo (Kiyota et al., 2008). It can achieve double amplitude shear strain levels (γ_{DA}) of 100% on medium-size hollow cylindrical specimens with a max height (H) of 300 mm and an outer diameter (D_o) of 200 mm. Full details of the apparatus can be found in Kiyota et al. (2008), while definitions of the stress and strain components are described in Chiaro et al. (2013b, 2017).

All the experiments were performed on Toyoura sand (specific gravity $Gs = 2.659$, maximum void ratio $e_{max} = 0.951$, minimum void ratio $e_{min} = 0.608$, and fines content $Fc < 0.1\%$). Its particle size distribution curve and a photo of a typical sub-angular grain are presented in Fig. 1. In this study, the specimen size of $H = 300$ mm, $D_o = 150$ mm, and inner diameter (D_i) = 90-mm were used for Tests No. 1 to 34, while the specimen size of $H = 200$ mm, $D_i = 100$ mm, and $D_i = 60$ mm were used for all the other tests. A list of all the tests performed is given in Table 2. Umar et al. (2018) showed that the undrained monotonic and cyclic deformation characteristics of Toyoura sand are essentially the same for these two specimen sizes.

For the specimen preparation, the air-pluviation technique proposed by Chiaro et al. (2012) was adopted. To assure a high degree of saturation, the specimens were kept under a double vacuum (Ampadu, 1991) for 1 h and then

Table 1
Density classification used in this study for Toyoura sand.

Density state	Void ratio/Relative density range
Very loose	$e_0 \geq 0.870$ ($D_r \leq 24\%$)
Loose	$e_0 = 0.830$–0.869 ($D_r = 24$–35%)
Medium-dense	$e_0 = 0.730$–0.829 ($D_r = 35$–65%)
Dense	$e_0 \leq 0.729$ ($D_r \geq 65\%$)

D_r: relative density and e_0: void ratio after consolidation.

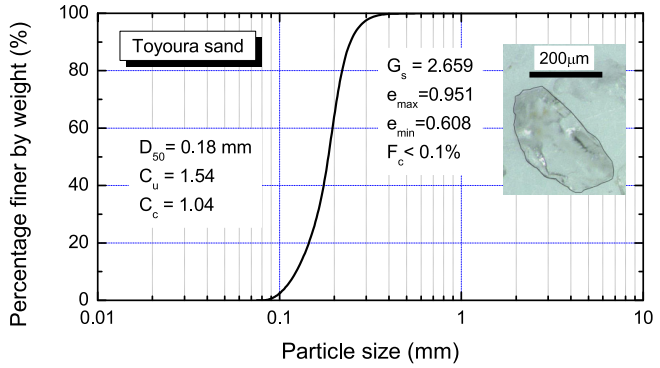

Fig. 1. Particle size distribution and microscopic view of typical sub-angular grain of Toyoura sand tested in this study.

de-aired water was circulated into the specimens. To improve the degree of saturation, a back pressure of 200 kPa was applied and Skempton's B-value was ensured to be ≥ 0.96. Finally, the specimens were isotropically consolidated to a mean effective principle stress (p'_0) of 100 kPa.

The sloping ground conditions were simulated by applying drained monotonic torsional shear stress on the specimens up to the desired level of static shear stress (see the summary in Table 2) before applying cyclic torsional shear loading under undrained conditions. The shear loading was applied at a constant strain rate of 0.1%/min, and the loading direction was reversed once the target cyclic shear stress value had been reached in one direction (which was corrected for the membrane force effects, as reported in Chiaro et al. (2021)). During the process of undrained torsional loading, the vertical displacement of the top cap was mechanically prevented in order to simulate quasi-simple shear conditions and to closely replicate the stress in the field during earthquake shaking (Kiyota et al., 2008).

2.1. Stress-reversal and stress-non-reversal loading conditions

As described schematically in Fig. 2, before earthquake shaking, the soil element beneath the sloping ground is subjected to initial static shear stress (τ_{static}) induced by the slope inclination conditions. During the earthquake shaking, the reference soil element undergoes partial or no shear stress reversal loading conditions due to the superimposition of seismically induced cyclic shear stress (τ_{cyclic}) to τ_{static}. When $\tau_{static} < \tau_{cyclic}$, the shear stress changes within the maximum positive value of τ_{max} ($=\tau_{static} + \tau_{cyclic}$) > 0 and the minimum negative value of τ_{min} ($=\tau_{static} - \tau_{cyclic}$) < 0 during each cycle of loading. This type of loading is known as stress-reversal (SR) or two-way loading. On the other hand, when $\tau_{static} > \tau_{cyclic}$, the shear stress is always positive (i.e., $\tau_{max} > 0$ and $\tau_{min} > 0$). This condition is called stress-non-reversal (SNR) or one-way loading (Yoshimi and Ohoka, 1975; Hyodo et al., 1991).

3. Test results

3.1. Undrained monotonic response with initial static shear

Fig. 3(a) and (b) show the undrained monotonic loading (ML) effective stress paths and stress–strain relationships following isotropic consolidation without the static stress ratio ($\alpha = \tau_{static}/p'_0 = 0$). For comparison, Fig. 3(c) and (d) show the effective stress paths and stress–strain relationships during the first quarter cycle of undrained cyclic loading (i.e., equivalent to undrained ML) for $\alpha = 0.20$. The tests were conducted under different initial void ratios (e_0) after consolidation ($p'_0 = 100$ kPa).

All the specimens initially showed a tendency to contract (i.e., a decrease in the p'_0 value) during which the shear stress increased to the transient undrained peak shear stress ($\tau_{t.peak}$). The peak point marks the initiation of unstable behavior since the shear stress drops with further shearing to a transient minimum value, as the phase transformation state (PTS) or quasi-steady-state (QSS), during which the specimen deforms under nearly constant shear stress (Verdugo and Ishihara, 1996). As soon as the shear stress reaches the PTS, a tendency to dilate (i.e., an increase in the p'_0 value) takes over and the effective stress paths follow the failure envelope line (Ishihara et al., 1975).

Based on numerical observations, Chiaro et al. (2013a) reported that, for any given e_0, the value of $\tau_{t.peak}$ increases with increasing α. This finding is experimentally confirmed in the present study. Moreover, it is found that for any given α, the $\tau_{t.peak}$ value also increases with increasing e_0. A summary of the $\tau_{t.peak}$ values obtained for various e_0 and $\alpha = 0$, 0.15, 0.20, and 0.30 is provided in Fig. 4. It should be noted that, in the case of dense specimens that did not exhibit a clear $\tau_{t.peak}$, the $\tau_{t.peak}$ was taken at the shear stress at the PTS. Although the data points may be scattered, they seem to indicate that, for each value of α, a linear correlation between $\tau_{t.peak}$ and e_0 can be established.

The phenomenon whereby the resistance of sand decreases with further shearing, after the shear stress reaches its peak values, is called strain-softening. In the case of sloping grounds, the strain-softening is more critical as any slight dynamic disturbance might initiate flow failure. The degree of strain-softening for soils with initial static shear was defined by the modified brittleness index, I'_B (Sivathayalan and Vaid, 2002). I'_B is defined by the equation shown in Fig. 5; it is the ratio of the difference between $\tau_{t.peak}$ and the minimum strength (taken at PTS) to the difference between $\tau_{t.peak}$ and τ_{static}.

For soils without strain-softening behavior, I'_B is assumed to be equal to zero, while $I'_B > 1.0$ indicates that the minimum strength following $\tau_{t.peak}$ is smaller than τ_{static}, which suggests a high level of damage susceptibility. The difference between the I'_B for specimens at various τ_{static} and e_0 levels is shown in Fig. 5. As is evident from this figure, the specimens strain-softened over a wide range of

Table 2
List of tests performed and/or analyzed in this study.

Test	Relative density D_r (%)	Void ratio e_0	Cyclic stress ratio (CSR = τ_{cyclic}/p'_0)	Static stress ratio ($\alpha = \tau_{static}/p'_0$)	Type of loading*	Comments
1	23.6	0.870	0.12	0	SR	This study
2	21.3	0.878	0.12	0.05	SR	
3	21.3	0.878	0.12	0.10	SR	
4	23.6	0.870	0.12	0.15	SNR	
5	22.2	0.875	0.12	0.20	SNR	
6	23.6	0.870	0.12	0.25	SNR	
7	29.8	0.849	0.12	0	SR	Chiaro et al. (2021)
8	28.9	0.852	0.12	0.05	SR	
9	25.6	0.864	0.12	0.10	SR	
10	25.8	0.863	0.12	0.15	SNR	
11	24.7	0.866	0.12	0.20	SNR	
12	27.7	0.856	0.12	0.25	SNR	
13	25.1	0.865	0.12	0.30	SNR	
14	24.1	0.869	0.16	0	SR	Umar et al. (2016)
15	25.7	0.863	0.16	0.05	SR	
16	25.6	0.864	0.16	0.10	SR	
17	29.8	0.849	0.16	0.15	SR	
18	28.1	0.855	0.16	0.20	SNR	
19	28.9	0.852	0.16	0.25	SNR	
20	24.1	0.868	0.16	0.30	SNR	
21	32.4	0.840	0.12	0.15	SNR	This study
22	32.4	0.840	0.12	0.20	SNR	
23	46.4+	0.825	0.16	0	SR	Chiaro et al. (2012)
24	45.5+	0.828	0.16	0.05	SR	
25	46.6+	0.824	0.16	0.10	SR	
26	44.2+	0.833	0.16	0.15	SR	
27	46.5+	0.825	0.16	0.16	SNR	
28	45.3+	0.829	0.16	0.20	SNR	
29	48.1+	0.819	0.20	0	SR	
30	48.0+	0.819	0.20	0.05	SR	
31	45.6+	0.828	0.20	0.10	SR	
32	44.4+	0.832	0.20	0.15	SR	
33	46.9+	0.823	0.20	0.20	SNR	
34	46.1+	0.826	0.20	0.25	SNR	
35	72.9	0.701	0.20	0	SR	This study
36	69.7	0.712	0.20	0.10	SR	
37	69.7	0.712	0.20	0.15	SR	
38	73.5	0.699	0.20	0.20	SNR	
39	70.0	0.711	0.30	0	SR	
40	73.2	0.700	0.30	0.10	SR	
41	73.5	0.699	0.30	0.20	SR	
42	73.8	0.698	0.30	0.30	SNR	
43	19.5	0.884	Monotonic	0	ML	This study
44	27.4	0.857	Monotonic	0	ML	
45	50.7	0.777	Monotonic	0	ML	
46	72.0	0.704	Monotonic	0	ML	
47	53.9	0.766	Monotonic	0.15	ML	

* SR: stress reversal, SNR: stress non-reversal, and ML: monotonic loading.
+ Different Toyoura sand batch ($e_{max} = 0.992$ and $e_{min} = 0.632$).

initial densities, and the I'_B of the sand increased with increasing τ_{static}. At $e_0 = 0.70$ ($D_r = 73\%$), the sand does not strain-soften with an increasing level of τ_{static}. This is contradictory to the observations made for silica sand with τ_{static} by Sivathayalan and Vaid (2002) and Sivathayalan and Ha (2011). They found that silica sand exhibited significant strain-softening with an increasing level of static shear even at $D_r = 70\%$. Soil particle angularity plays a key role in determining the strain-softening response of soils, as highlighted by Sivathayalan and Ha (2011). The difference in the strain-softening responses between Toyoura and silica sand could, therefore, be associated with the particle angularity, as both types of sand have identical mean diameters and particle gradations.

The plot in Fig. 5 indicates that the degree of strain-softening of Toyoura sand depends on the static shear level. For instance, at $e_0 = 0.850$, I'_B is about 0.6 for $\alpha = 0$ and becomes 2.5 for $\alpha = 0.15$ and 4.5 for $\alpha = 0.30$.

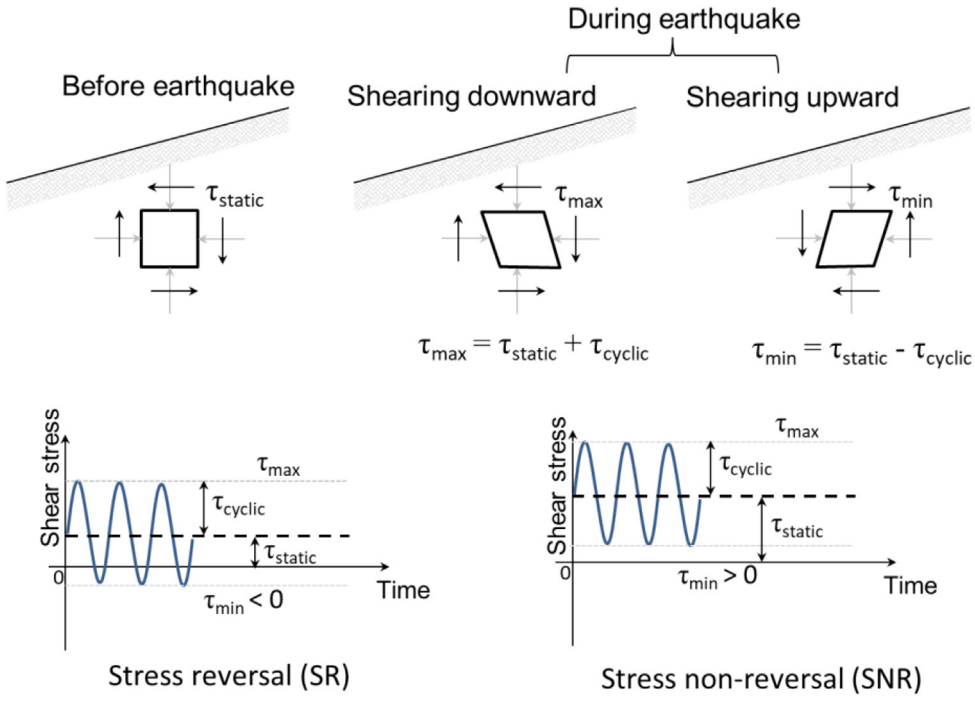

Fig. 2. Stress reversal (SR) and stress non-reversal (SNR) loading conditions in sloping ground during earthquake (). adopted from Chiaro et al., 2013a

3.2. Undrained cyclic response under initial static shear

Typical effective stress paths and stress–strain relationships for very loose ($e_0 = 0.878$) and loose ($e_0 = 0.852$) Toyoura sand specimens subjected to SR loading conditions are shown in Fig. 6, while those for medium dense ($e_0 = 0.828$) and dense ($e_0 = 0.712$) specimens are shown in Fig. 7.

The effective stress paths and stress–strain relationships for very loose ($e_0 = 0.870$) and loose ($e_0 = 0.863$) specimens subjected to SNR loading conditions are presented in Fig. 8, while those for medium dense ($e_0 = 0.829$) and dense ($e_0 = 0.699$) specimens are presented in Fig. 9.

3.2.1. Stress reversal (SR) ($\tau_{cyclic} > \tau_{static}$)

For the very loose specimen ($e_0 = 0.878$), a gradual shear strain developed during cyclic loading until the 18th loading cycle. In the subsequent cycle, the specimen eventually reached the state of zero mean effective principal stress ($p'_0 = 0$) or the full liquefaction state, as shown in Fig. 6(a). Simultaneously, the specimen also achieved a state of zero shear stress, as is evident from the stress–strain plot shown in Fig. 6(b). Photo 1 presents photos of the sand specimen deformation at state A (after consolidation and before shearing) and state B (state of zero shear stress during shearing), reported for completeness. The photo of state B suggests that the upper region of the specimen "collapsed" due to a complete loss of shear strength in the specimen. Yet, the specimen continued to deform under the state of zero shear stress until the shear strain of about 27% was reached. After that, the shear resistance of the sand gradually started to increase. This implies that even the loosest sand will recover its stiffness and strength at large shear strain levels, thus preventing further shear deformation. This finding is consistent with earthquake-induced flow failure observations whereby the sand essentially reaches a standstill after developing large deformation due to the dissipation of excess pore water pressure or the geometrical non-linearity of the soil wedge formed by the flow.

As shown in Fig. 6(c) and (d), in the case of the loose specimen ($e_0 = 0.852$), the effective stress path and stress–strain behavior are distinct from those of the very loose specimen. Cyclic mobility was observed in the effective stress path where the effective stress recovered repeatedly after reaching the state of $p'_0 = 0$. It was accompanied by a significant development of shear strain, as can be observed by the stress–strain relationship in Fig. 6(d).

For the medium-dense ($e_0 = 0.828$) and dense specimens ($e_0 = 0.712$) shown in Fig. 7, the deformation modes of the effective stress paths and the stress–strain responses are similar to those of the loose specimen (i.e., cyclic mobility-induced deformation). Yet, the rate of development of shear strain with each loading cycle is less than that of the loose specimen. At the same amplitude of τ_{max}, the medium dense specimen showed monotonic-like behavior as the applied stress exceeded $\tau_{t.peak}$, whereas the dense specimen showed typical cyclic behavior before reaching the state of $p'_0 = 0$. This is natural and expected as higher density results in higher $\tau_{t.peak}$, as discussed in detail in Section 3.1.

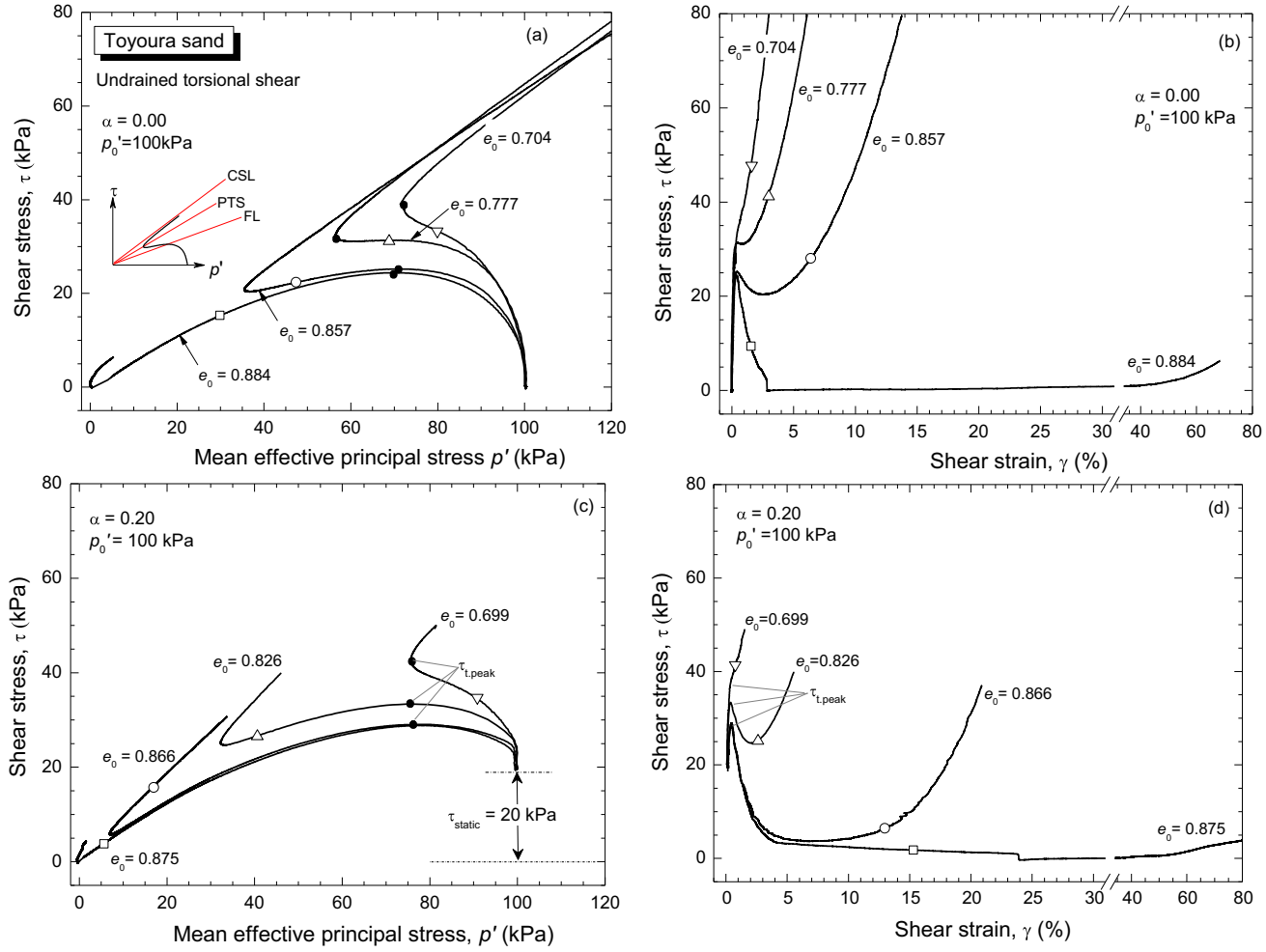

Fig. 3. Toyoura sand responses in undrained monotonic torsional shear tests with and without initial static shear.

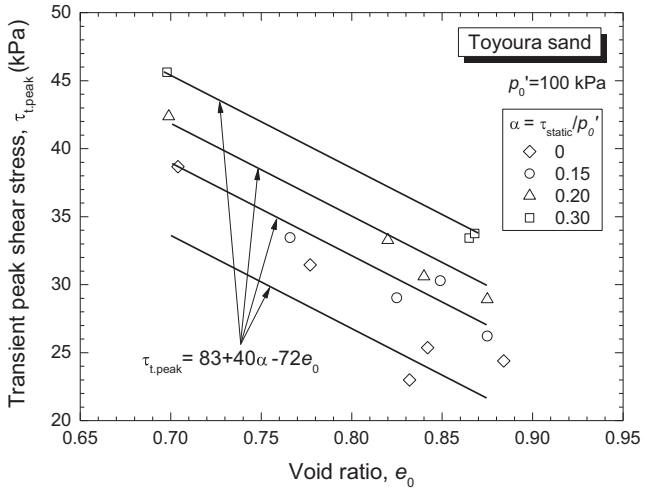

Fig. 4. Effects of void ratio and shear stress ratio on transient undrained peak shear stress of Toyoura sand in undrained torsional shear tests.

3.2.2. Stress Non-Reversal (SNR) ($\tau_{static} > \tau_{cyclic}$)

The effective stress paths and stress–strain responses for very loose ($e_0 = 0.870$) and loose ($e_0 = 0.863$) specimens are different under SNR conditions (Fig. 8) as well.

For the very loose specimen, the behavior did not change after $p_0' = 0$ under either SR or SNR loading conditions (i.e., the specimen showed an abrupt flow-type behavior after achieving $p_0' = 0$). However, under SNR loading conditions, the very loose specimen exhibited static liquefaction instead of cyclic liquefaction because τ_{max} ($=\tau_{cyclic} + \tau_{static}$) exceeded $\tau_{t.peak}$. Such a response of the specimen is consistent with static liquefaction typically observed under undrained monotonic shear loading without static shear, as presented in Section 3.1.

As shown in Fig. 8(c) and (d), the response of the loose specimen is different from that of the very loose specimen. The state of $p_0' = 0$ was not achieved and deformation accumulated progressively until reaching a state of strain local-

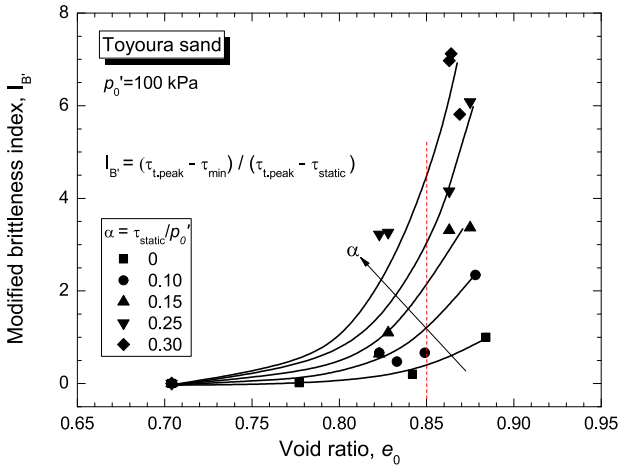

Fig. 5. Effects of void ratio and shear stress ratio on modified brittleness index of Toyoura sand in undrained torsional shear tests.

ization or non-uniform deformation (Kiyota et al., 2008). Chiaro et al. (2013b) and Umar et al. (2016b) showed that, at large strain under SNR, the failure resulted from the development of a shear band(s) in the specimen.

On the other hand, as shown in Fig. 9, the medium-dense ($e_0 = 0.820$) and dense ($e_0 = 0.699$) specimens exhibited deformation modes comparable to that of the loose specimen. Progressive deformation accumulated with each loading cycle at a rate of 0.45% for the medium-dense specimen and 0.05% for the dense specimen. The results show that the deformation continued to develop in the medium-dense specimen up to the large strain of $\gamma_{SA} > 50\%$, while in the dense specimen, the deformation was unable to develop despite repeated cyclic shearing. This highlights the importance of the density state and implies that the denser sand will develop limited deformation under SNR.

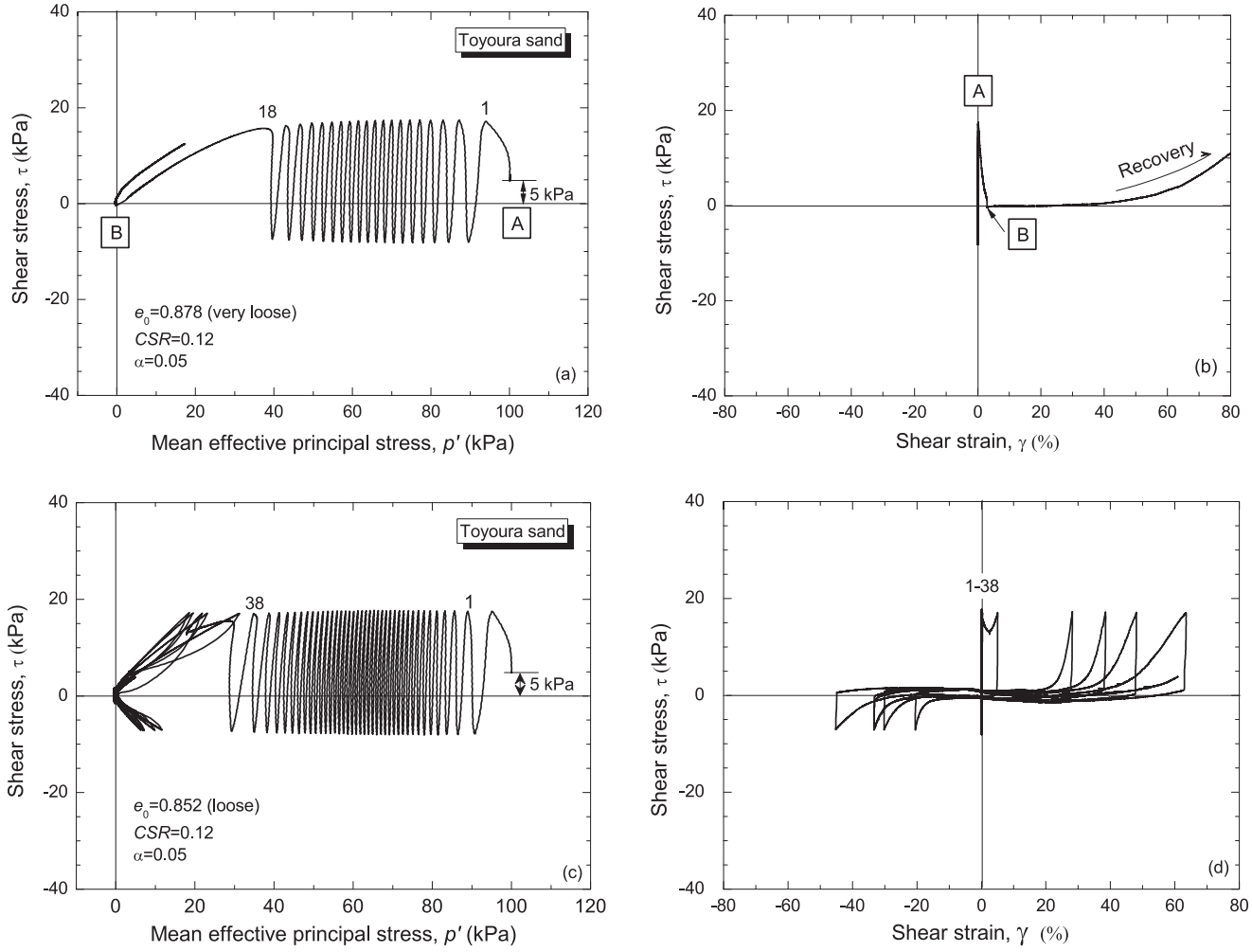

Fig. 6. Undrained cyclic torsional shear responses of very loose ($e_0 = 0.878$) and loose ($e_0 = 0.852$) Toyoura sand under stress reversal loading conditions ($CSR = 0.12$; $\alpha = 0.05$).

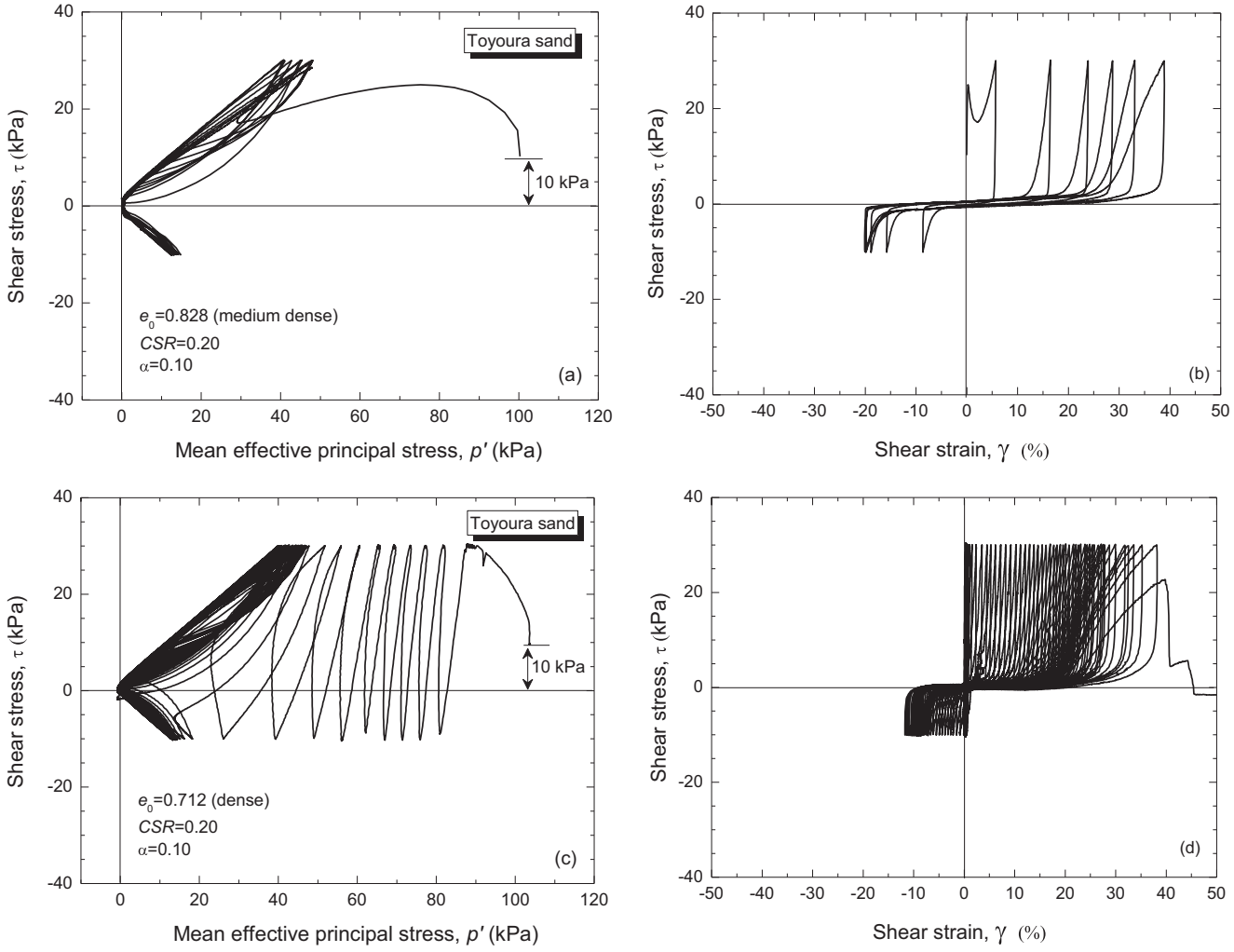

Fig. 7. Undrained cyclic torsional shear responses of medium-dense ($e_0 = 0.828$) and dense ($e_0 = 0.712$) Toyoura sand under stress reversal loading conditions ($CSR = 0.20$; $\alpha = 0.10$).

3.3. Classification of deformation modes

Fig. 10 shows a schematic illustration of the undrained shear responses of two specimens consolidated at loose and dense states, as indicated by 1 and 2. Sand 1 (dense), having a void ratio (e_0) less than the critical void ratio (e_c is defined in this study as the void ratio at which the sand shows zero residual strength), will first achieve the phase transformation state, due to its tendency to contract during shearing, and then the ultimate steady state (i.e., critical state) after fully mobilizing positive dilatancy (Murthy et al., 2007). Sand 2 (loose), having a void ratio (e_0) more than the critical void ratio (e_c), will tend to contract and strain-soften throughout the entire shearing phase. The ultimate steady state can eventually be achieved in very loose sand only after large deformation (e.g., Fig. 6(b)). It is well established that saturated sands show zero dilatancy at a void ratio equal to e_c when subjected to undrained loading (Casagrande, 1965; Robertson and Fear, 1995).

In the present study, the mode of deformation in the presence of initial static shear (τ_{static}) is in accordance with previous studies for very loose sand and in conflict with them for loose sand, even though the difference in their density states may be marginal. This suggests that loose sand cannot always be associated with flow-type behavior. To improve our understanding, it is essential to identify the mode of deformation based on widely accepted parameters, such as the consolidated void ratio (e_0) and transient undrained peak shear stress ($\tau_{t.peak}$). A thorough examination of the results of tests on very loose to dense specimens revealed the existence of five possible deformation modes.

The first failure mode, referred to hereafter as *static liquefaction,* has been typically observed in very loose sand ($e_0 \geq e_c$) for SNR loading conditions and $\tau_{cyclic+} \tau_{static} > \tau_{t.peak}$. Fig. 11 shows the relationship between the accumulated shear strain ($\Sigma\gamma = \int|d\gamma/dt|\dot{s}dt$) and the excess pore water pressure ratio ($r_u = p'/p'_0$) for three very loose specimens. Such deformation is similar to that observed in very loose sand under monotonic loading without static shear

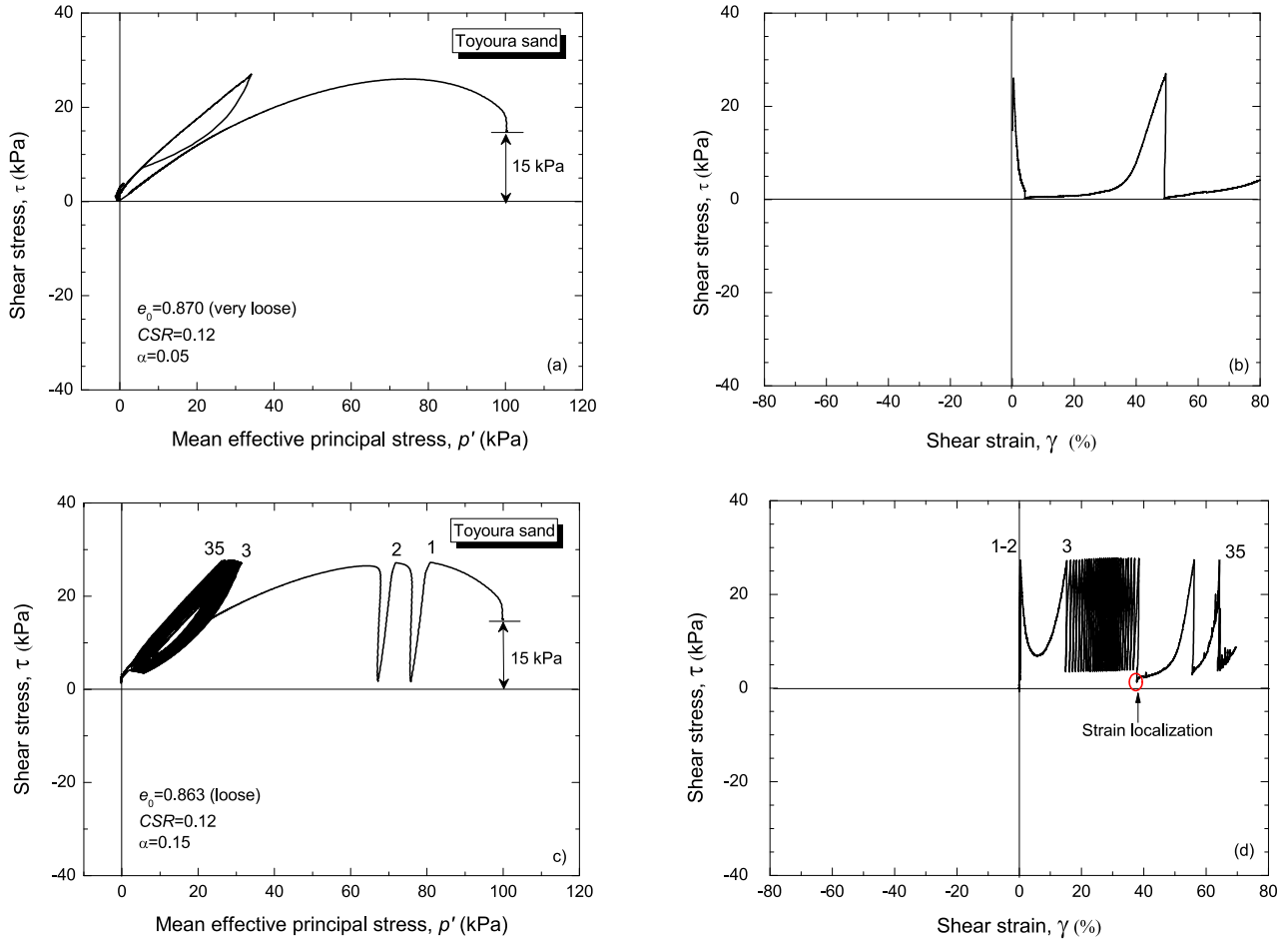

Fig. 8. Undrained cyclic torsional shear responses of very loose ($e_0 = 0.870$) and loose ($e_0 = 0.863$) Toyoura sand under stress non-reversal loading conditions ($CSR = 0.12$; $\alpha = 0.05$–0.15).

(e.g., Yang, 2002; Been & Jefferies, 2004; Umar et al., 2019). It is categorized by the rapid buildup of excess pore water pressure (EPWP) and large deformation upon reaching $r_u = 1.0$ without the significant development of $\Sigma\gamma$. The sand will recover its strength and stiffness after mobilizing particle–particle interlocking at large shear deformation.

The second failure mode, referred to hereafter as *cyclic liquefaction*, is applicable to very loose sand ($e_0 \geq e_c$) when $\tau_{t.peak} > \tau_{cyclic} + \tau_{static}$ under SR loading conditions (Fig. 11). For the cyclic liquefaction mode, a progressive development of EPWP with $\Sigma\gamma$ is observed. The failure mode is characterized by runaway deformation once it is achieved at a state of $r_u = 1.0$ (i.e., full liquefaction state).

Fig. 12 shows the third deformation mode, in terms of r_u and $\Sigma\gamma$, that is well known as *cyclic mobility*. It has been observed in loose to dense sand ($e_0 < e_c$) when $\tau_{cyclic} > \tau_{static}$ (under SR loading conditions) and $\tau_{t.peak} < \tau_{cyclic} + \tau_{static}$. Previous studies reported cyclic mobility in sand at $Dr \sim 50\%$ (e.g., Yang et al., 2011). However, as Fig. 12 shows, even a loose specimen ($D_r = 25\%$) may show cyclic mobility under SR loading conditions.

In the case of $\tau_{cyclic} < \tau_{static}$ (SNR loading) and $e_0 < e_c$, the *shear deformation* or *cyclic strain accumulation* mode (without $p_0' = 0$ state) takes over, as shown in Fig. 13. However, as the sand density increases (from medium-dense to dense), the development of shear strain during cyclic loading becomes limited and the fifth deformation mode, hereafter referred to as *limited shear deformation,* will take place.

A graphical method for identifying/predicting each mode of deformation is proposed in Fig. 14. It consists of a stress ratio-void ratio plot, for which the static liquefaction zone, cyclic liquefaction zone, cyclic mobility zone, shear deformation zone, and limited deformation zone are clearly defined. In the plot, factor β is defined by the following equation:

$$\beta = \frac{\tau_{static}}{\tau_{cyclic}} \times \frac{\tau_{t.peak}}{p_0'} \quad (1)$$

Factor β is an indicator of how the combination of τ_{static}, τ_{cyclic}, $\tau_{t.peak}$, and p_0' influences the mode of deformation depending on the sand density state. Eq. (1) has been selected so that when $\tau_{static} = \tau_{cyclic}$ (reversal loading line), the plot shown in Fig. 14 corresponds to that shown in Fig. 4 and well-defined $\tau_{t.peak}$ lines can be established. Moreover, for the same combination of e_0 and α values,

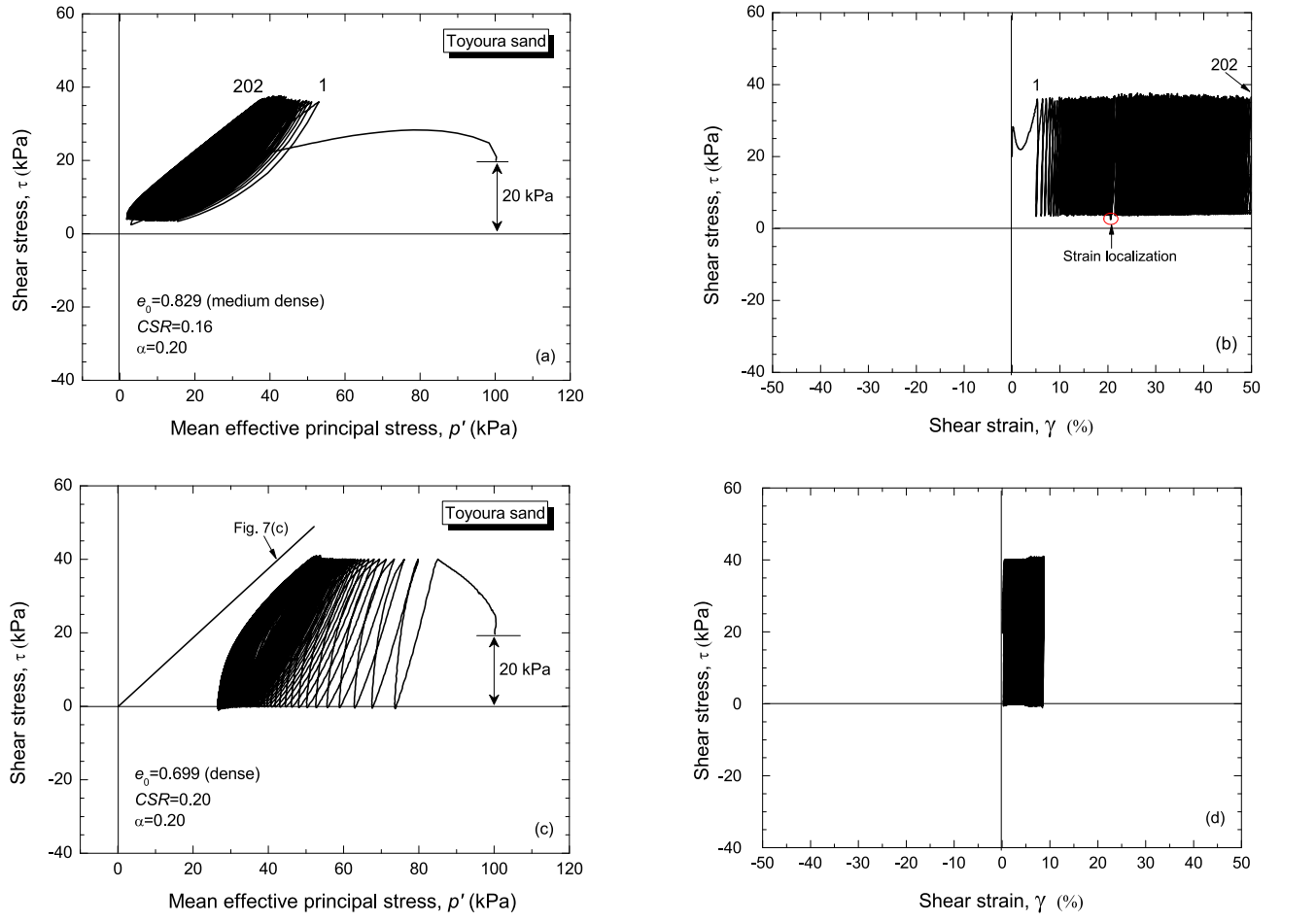

Fig. 9. Undrained cyclic torsional shear responses of medium-dense ($e_0 = 0.829$) and dense ($e_0 = 0.699$) Toyoura sand under stress non-reversal loading conditions ($CSR = 0.16$–0.20; $\alpha = 0.20$).

a β value below the $\tau_{t.peak}$ line indicates the SR loading conditions, while a β value above the $\tau_{t.peak}$ line indicates the SR loading conditions.

More specifically, for a value of β below any given $\tau_{t.peak}$ line, the sand will exhibit cyclic mobility if $e_0 < e_{c.}$ (loose to dense sand) or cyclic liquefaction if $e_0 \geq e_{c.}$(very loose sand). The mode of deformation changes to shear deformation and limited deformation for β above the $\tau_{t.peak}$ line and $e_0 < e_c$; otherwise, for $e_0 \geq e_c$, the static liquefaction failure mode will occur. It should be noted that the region between shear deformation and limited deformation has been tentatively defined based on the fact that specimens with $e_0 \leq 0.729$ do not show a clear transient undrained shear stress peak state ($\tau_{t.peak}$) followed by limited flow deformation (see the dense specimen behavior shown in Fig. 3).

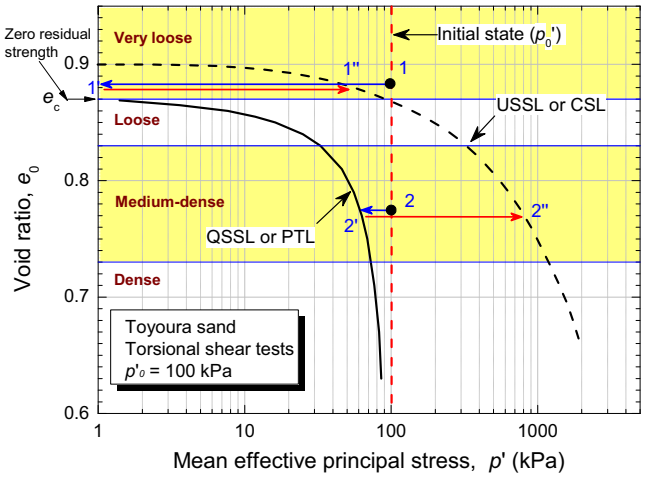

Fig. 10. Undrained shear behavior of Toyoura sand in torsional shear tests – QSS: quasi-steady state, PT: phase transformation, USS: ultimate-steady state, and CS: critical state (adopted from Yoshimine and Ishihara 1998).

4. Resistance against cyclic strain accumulation

4.1. Strain accumulation criteria

Liquefaction resistance or cyclic strain accumulation is usually expressed by the cyclic stress ratio ($CSR = \tau_{cyclic}/p'_0$) required to develop a particular amount of deformation during cyclic loading (i.e., single, γ_{SA}, or double amplitude

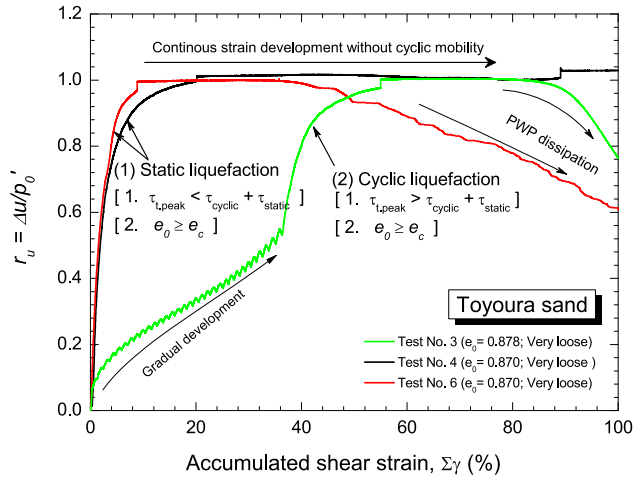

Fig. 11. Static liquefaction and cyclic liquefaction failure types typically observed for Toyoura sand in torsional shear tests with initial static shear.

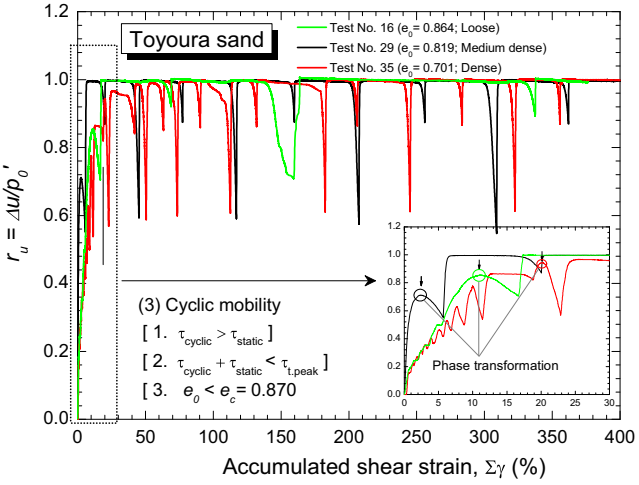

Fig. 12. Cyclic mobility failure type typically observed for Toyoura sand in stress reversal torsional shear tests.

shear strain, γ_{DA}). However, due to the presence of initial static shear (τ_{static}), shear strain accumulates in the direction of the applied initial static shear and becomes unsymmetrical. Therefore, γ_{DA} may not accurately represent the strain accumulation during cyclic loading with τ_{static} (Chiaro et al., 2012; 2020). Therefore, following the study of Chiaro et al. (2012), the liquefaction resistance curves are described in this study in terms the static stress ratio ($\alpha = \tau_{static}/p'_0$) for γ_{SA} evaluated at the maximum shear stress state (γ_{SA} at $\tau = \tau_{max}$), as illustrated in Fig. 15. Moreover, the resistance against liquefaction (or more precisely, the resistance to strain accumulation) was evaluated in terms of the number of cycles required to develop a specific amount of γ_{SA} for both stress reversal and non-reversal loading conditions.

4.2. Cyclic resistance of sand with static shear

In this section, the development of strain accumulation for small ($\gamma_{SA} = 3\%$), moderate ($\gamma_{SA} = 7.5\%$), and large ($\gamma_{SA} = 20\%$) strain levels is compared for the different initial density states (from very loose to dense) with an increasing amplitude of α.

Fig. 16 compares the strain accumulation resistance required to achieve small, moderate, and large strain for very loose and loose specimens for $CSR = 0.12$. It can be seen in the figure that the strain accumulation resistance for small strain decreases from about 40 cycles of loading (at $\alpha = 0$, i.e., level ground condition) down to a half-cycle of loading or less when the α exceeds the CSR (i.e., SNR loading conditions). The strain accumulation resistance for moderate strain matches that for very loose and loose sand under the SNR loading conditions. This is because moderate strain development occurs in just a half-cycle of loading. On the contrary, for large strain, the cyclic resistance of loose sand first decreases from 42 cycles (at $\alpha = 0$) to 3.5 cycles (at $\alpha = 0.20$), and then increases slightly to 8 cycles (at $\alpha = 0.30$), indicating that the presence of τ_{static} is not always unfavorable.

Similarly, Fig. 17 compares the cyclic strain resistance of loose and medium-dense specimens for different levels of γ_{SA} for $CSR = 0.16$. The results indicate that, in the case of small and moderate strain levels, the cyclic strain accumulation resistance decreases with an increase in α. At a larger strain level, the cyclic resistance first decreases for $CSR < \alpha$ and then increases for $CSR > \alpha$. In Fig. 18, the comparison of cyclic strain resistance between medium-dense and dense specimens at $CSR = 0.20$ indicates that the strain accumulation resistance increases for dense specimens even before SNR has been achieved.

Thus, these tests suggest that the level of shear strain at which the resistance against stain accumulation is defined plays an important role in the evaluation of the effect of τ_{static} on the strain accumulation resistance, as was also suggested by Chiaro et al. (2012, 2020) and Umar et al. (2016a, 2017). A combination of small to high strain levels,

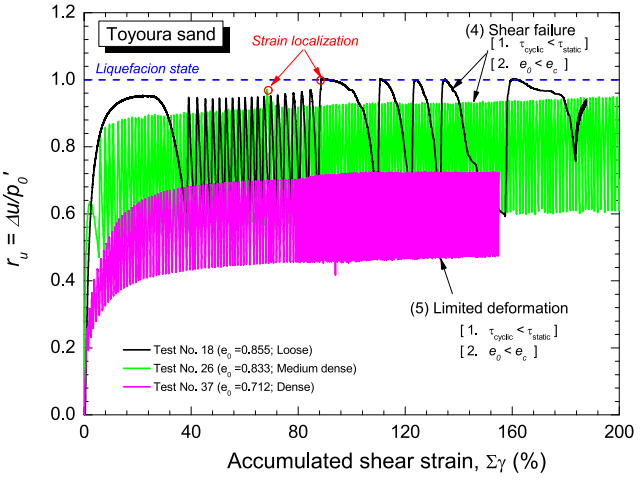

Fig. 13. Shear deformation and limited deformation behavior typically observed for Toyoura sand in stress reversal torsional shear tests.

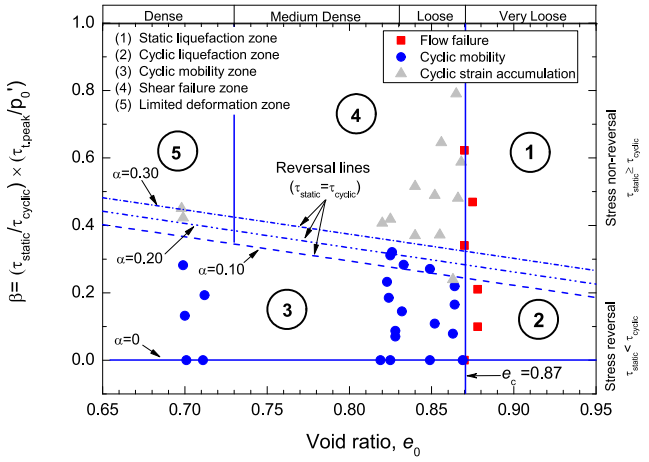

Fig. 14. Behavioral failure zones for Toyoura sand in torsional shear tests with initial static shear.

used to define the cyclic resistance, together with the initial density state, would provide a better understanding of the typical two-phase change (i.e., first a decrease and then an increase) of the cyclic strain resistance of sand subjected to τ_{static}.

Fig. 19 shows the cyclic resistance of dense sand for small and moderate strain in the presence of initial static shear, while that for loose and medium-dense sand has already been reported in Chiaro et al. (2021). The cyclic resistance curves given in Fig. 20 show that the density state required to resist the equivalent cyclic stress ratio due to a magnitude M_w7.5 earthquake, is expected to produce 10 stress cycles (Seed et al., 1975). The cyclic resistance ratio versus α relationships are illustrated in Fig. 20 for small, moderate, and large strain levels. They allow for the determination of the K_α correction factor at various levels of shear strain. K_α is defined by the following equation (Seed, 1983):

$$K_\alpha = \frac{CRR_\alpha}{CRR_{\alpha=0}} \quad (2)$$

where the cyclic stress ratio (CRR) refers to the CSR required to cause shear strain in 10 loading cycles, CRR_α is the CRR value for a given value of α, and $CRR_{\alpha=0}$ is the CRR value when $\alpha = 0$ (level ground).

The value of K_α indicates when the presence of static shear is detrimental ($K_\alpha < 1$) or beneficial ($K_\alpha > 1$) to the sand's cyclic resistance. Sivathayalan and Ha (2011) showed that the effect of K_α mainly depends on the material type. In other words, for strain-softening sands, K_α will be much smaller than 1, while for strain-hardening sands, K_α will be>1. However, the material response can be different at different strain levels. In this study, therefore, K_α is defined at and compared for different shear strain levels.

Fig. 21 presents the variation in K_α with α obtained in this study for Toyoura sand for various density states and $p'_0 = 100$ kPa for small, moderate, and large strain levels. The test results of Sivathayalan and Ha (2011) are also plotted for comparison.

Fig. 21(a) shows that, at small strain, the loose sand resistance quickly decreases with increasing α. For $\alpha = 0.2$, the loose sand possesses only 40% of the cyclic resistance as compared to the case of $\alpha = 0$. Yet, when the strain level increases from small to large (Fig. 21(c)), for $\alpha = 0.2$, the same loose sand possesses about 60% of cyclic resistance as compared to the sand without static shear stress.

Alternatively, in the case of dense sand, the cyclic resistance first decreases and then increases with increasing α (Fig. 21(a) and (b)). At $\alpha = 0.1$, the cyclic resistance is about 80–90% as compared to the case of $\alpha = 0$, but then it increases and eventually exceeds that measured for $\alpha = 0$.

Fig. 21(a) also shows that τ_{static} decreased the cyclic resistance of silica sand among the different density states (i.e. loose, medium-dense, and dense). The trends for K_α are contradictory for silica and Toyoura sand at the dense state. Such inconsistent behavior can be associated with softening induced by particle angularity among sands, as highlighted by Sivathayalan and Ha (2011). Looking at the K_α responses for loose and medium-dense silica sand,

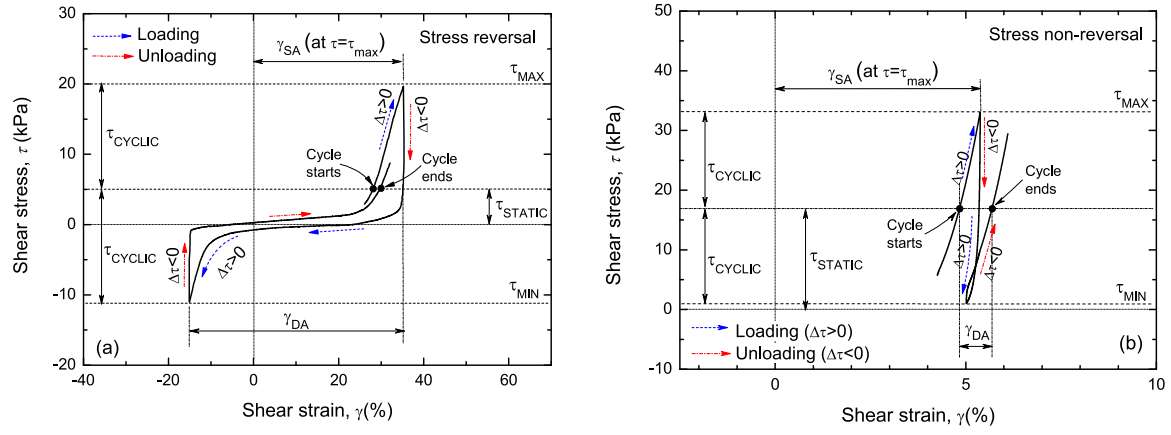

Fig. 15. Definition of shear strain components used in this study: (a) stress reversal and (b) non-reversal loading conditions (adopted from Chiaro et al., 2012).

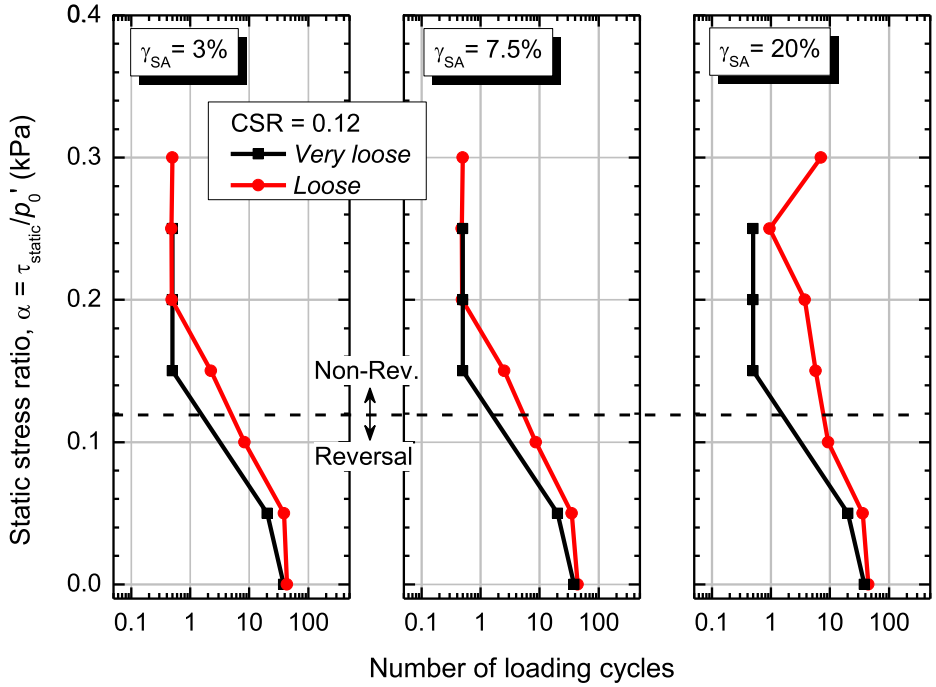

Fig. 16. Cyclic resistance of loose and very loose Toyoura sand at various shear strain levels: a) γ_{SA} = 3%, b) γ_{SA} = 7.5%, and c) γ_{SA} = 20%.

the static shear effect is detrimental to cyclic resistance. In the present study, however, even the loose sand showed a beneficial effect of static shear at a higher strain level. This reaffirms that the influence of static shear varies with the strain level. The conclusions based merely on a small strain level are insufficient to properly address the effect of initial static shear on the cyclic resistance of sand. Moreover, it has been widely reported that the influence of the fabric contributes to the cyclic resistance at a small strain level. Therefore, the sand response at a large strain level might be better representative due to the disappearance of inherent anisotropy.

5. Conclusions

In this paper, extensive large-strain undrained cyclic torsional simple shear tests with initial static shear were conducted on very loose to dense Toyoura sand specimens to

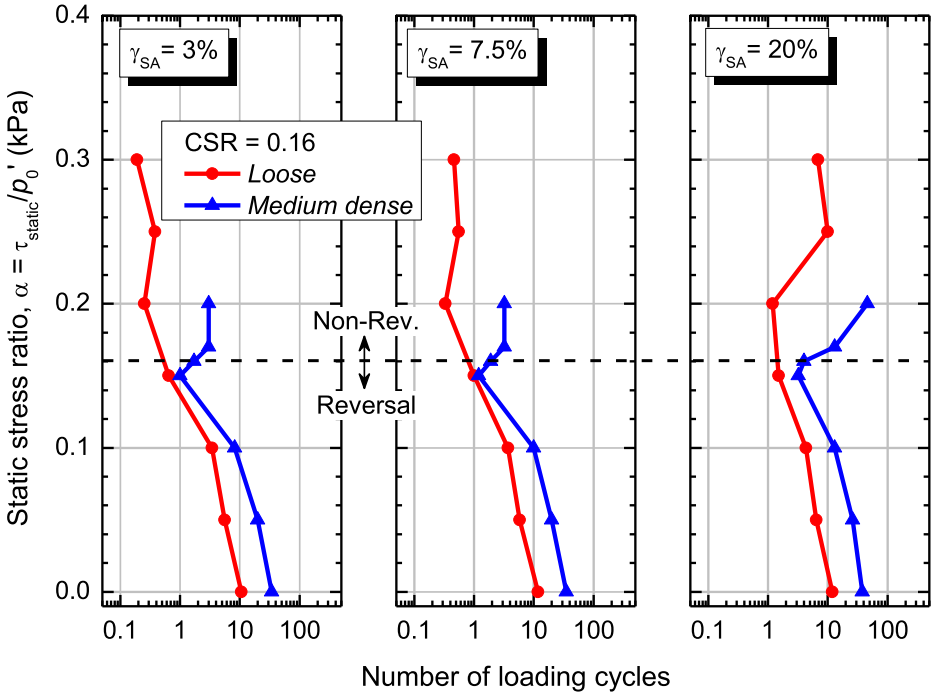

Fig. 17. Cyclic resistance of loose and medium-dense Toyoura sand at various shear strain levels: a) γ_{SA} = 3%, b) γ_{SA} = 7.5%, and c) γ_{SA} = 20%.

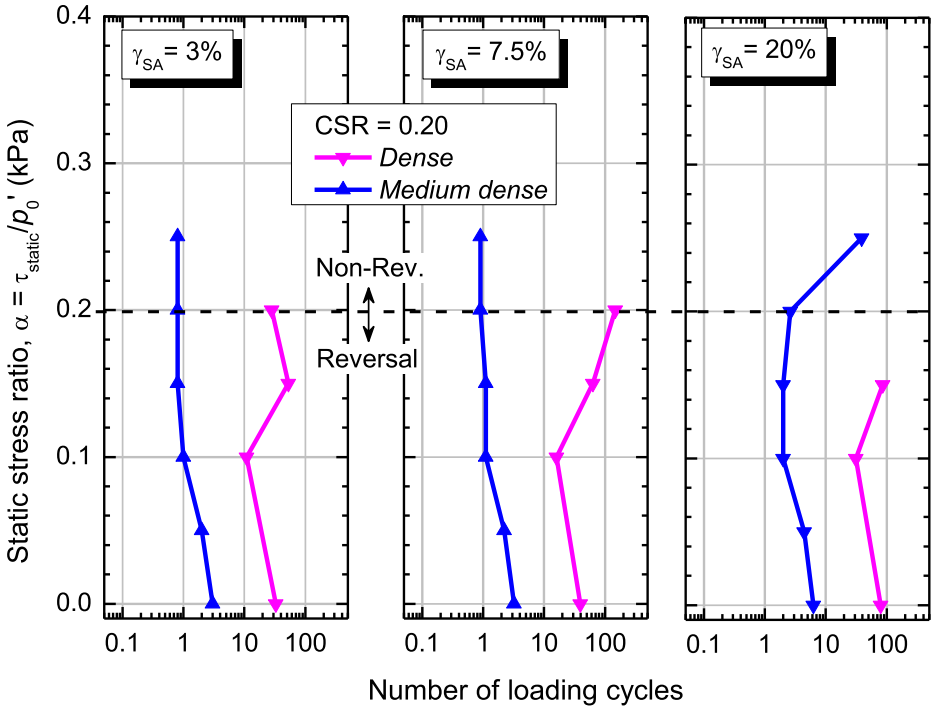

Fig. 18. Cyclic resistance of medium-dense and dense Toyoura sand at various shear strain levels: a) $\gamma_{SA} = 3\%$, b) $\gamma_{SA} = 7.5\%$, and c) $\gamma_{SA} = 20\%$.

provide a comprehensive understanding of the cyclic flow deformation response of liquefied sand subjected to sloping ground conditions. The following main conclusions can be drawn from this study:

(1) Under simple shear conditions, the sands in a sloping ground may experience five distinct failure mechanisms during earthquakes, namely, static liquefaction, cyclic liquefaction, cyclic mobility, shear deformation, and limited deformation failure. Such deformation modes can be predicted if the density state, transient undrained peak stress, and a combination of cyclic and static stresses are known. Cyclic liquefaction and static liquefaction occur in very loose sand. However, cyclic liquefaction will occur when the combined (static and cyclic) shear stress is less than the shear strength of the sand at the transient peak, while static liquefaction will occur when the soil strength is lower than the combined applied shear stress. The most critical failure mechanism is static liquefaction failure which produces an abrupt development of large shear deformation without any warning within a single loading cycle in loose sand. On the other hand, for loose to dense sand, failure is induced by cyclic mobility under stress reversal loading conditions, and shear deformation will take

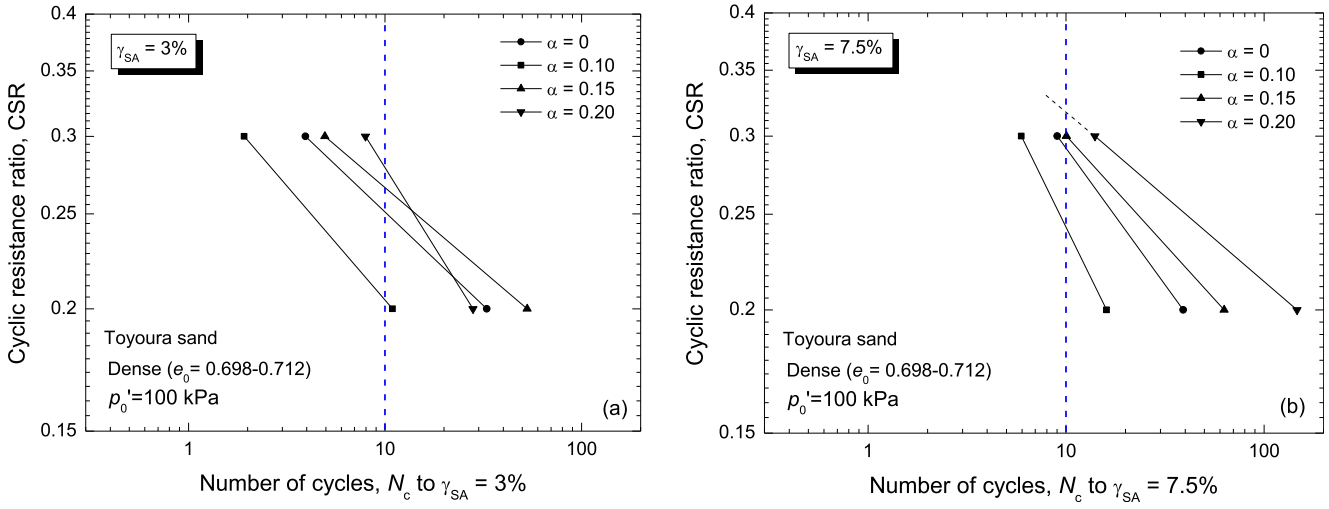

Fig. 19. Relationships between *CSR* and N_c for $\gamma_{SA} = 3, 7.5\%$ for dense Toyoura sand evaluated by undrained cyclic torsional shear tests with initial static shear.

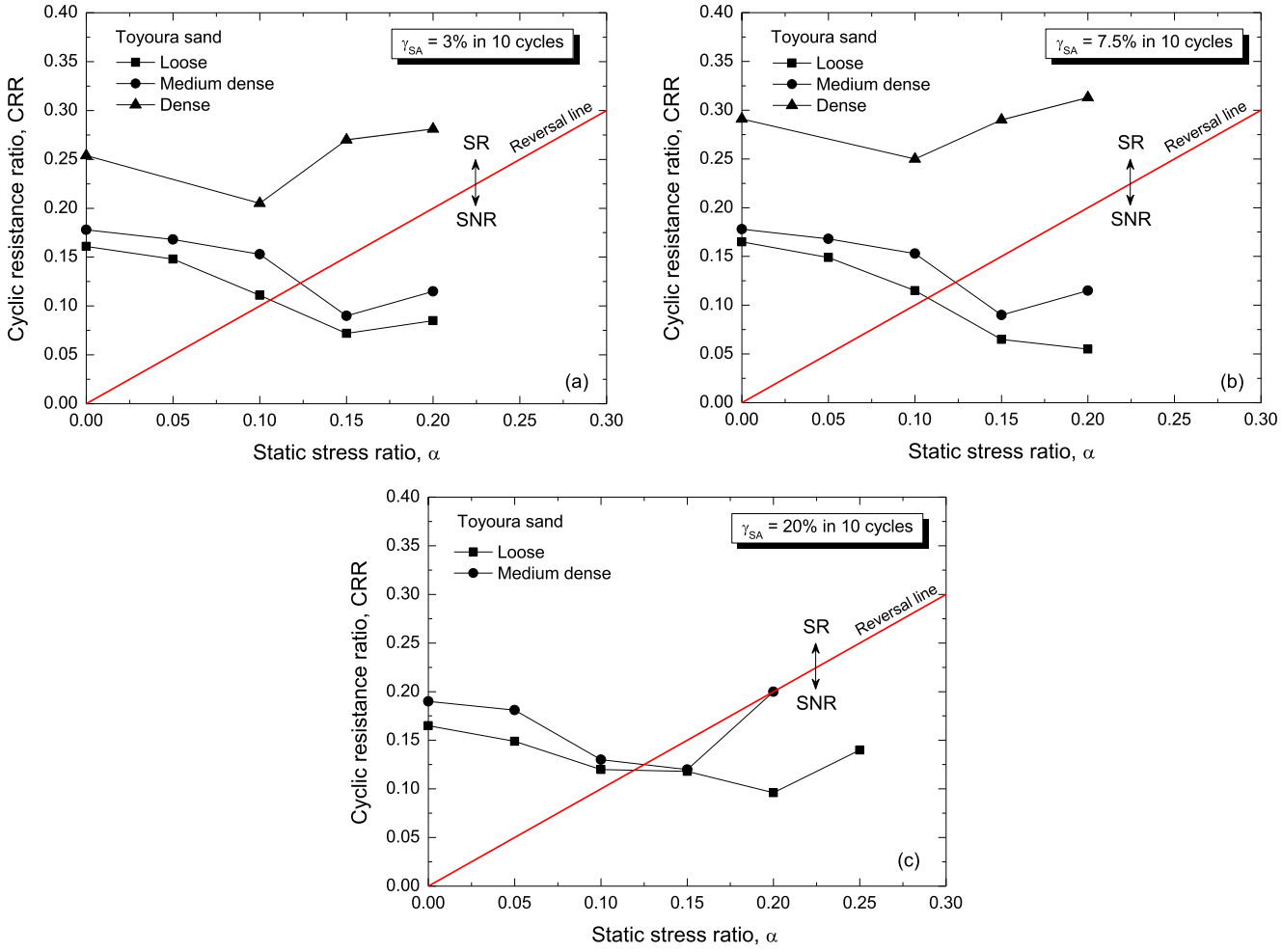

Fig. 20. Relationships between *CRR* and α for γ_{SA} = 3, 7.5, 20% (10 cycles of loading) evaluated by undrained cyclic torsional shear tests with initial static shear.

place under stress non-reversal loading conditions. The combination of cyclic and static stresses will govern the failure criteria.

(2) It was demonstrated that the presence of initial static shear is detrimental to the sand cyclic resistance for small (γ_{SA} = 3%), moderate (γ_{SA} = 7.5%), and large (γ_{SA} = 20%) strain levels for very loose sand, whereas it is detrimental for small and moderate strain levels, and beneficial at a large strain level for loose to dense sand.

(3) In this study, a comparison was made of K_α evaluated at small to large strain levels for different density states. The K_α value suggests that the cyclic resistance of very loose soil deteriorated from 1 to 0.4 for small strain and to 0.6 for moderate strain. The K_α value of dense soil increased from 1 to 1.2 with an increase in the strain level from small to moderate. The comparison among different strain levels suggests that the use of moderate to large strain levels would be preferable for quantifying the cyclic resistance of sand rather than the small strain level alone.

Acknowledgments

The first author would like to acknowledge the Asian Development Bank for providing a Ph.D. scholarship to study in the Civil Engineering Department of the University of Tokyo. The authors also acknowledge the technical assistance provided by Toshihiko Katagiri, Technical

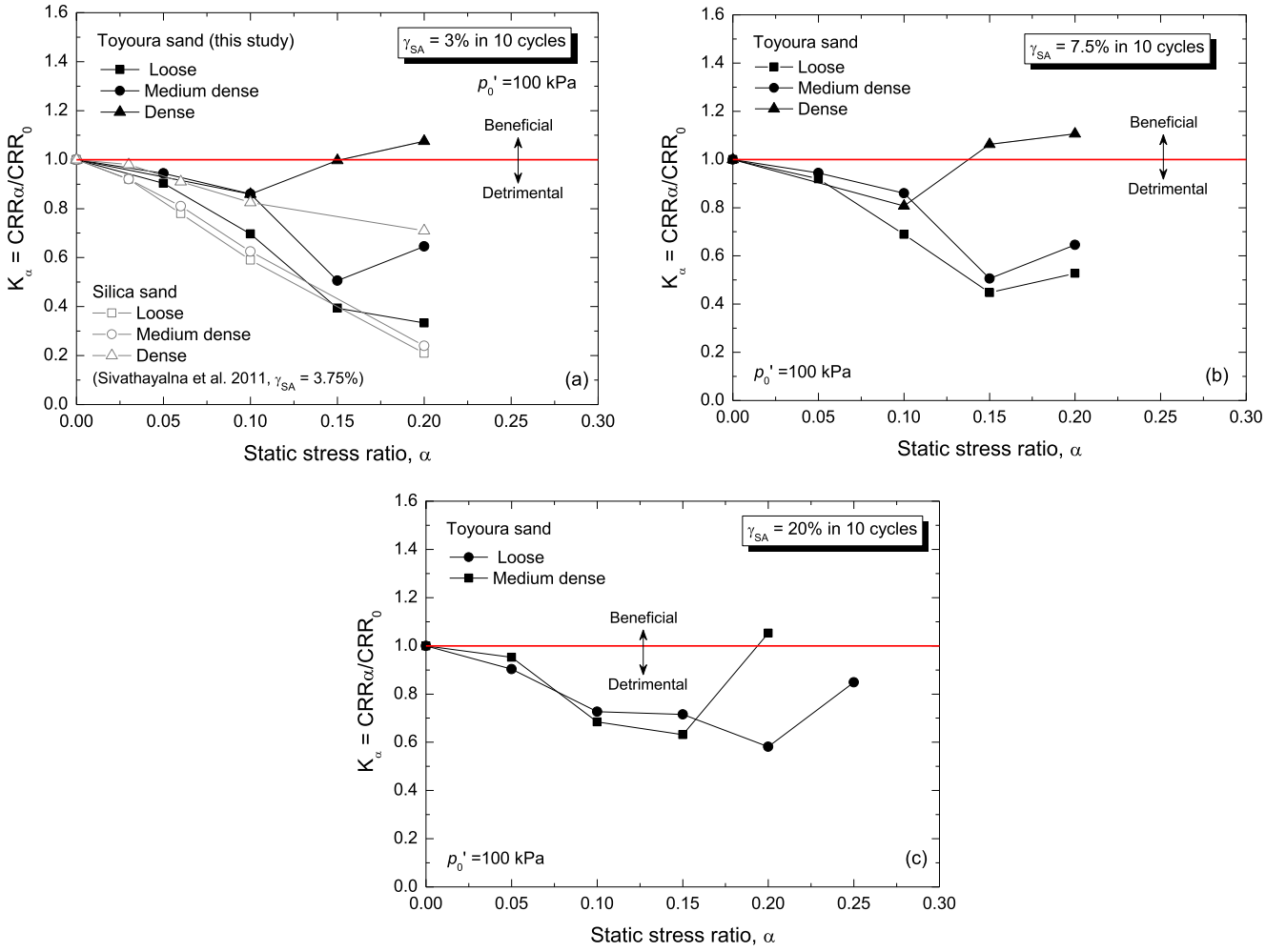

Fig. 21. Relationships between K_α and α for γ_{SA} = 3, 7.5, 20% (10 cycles of loading) evaluated by undrained cyclic torsional shear tests with initial static shear.

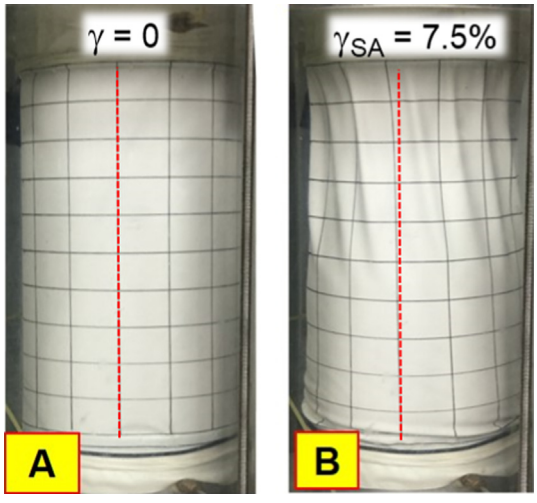

Photo 1. Specimen deformation of very loose (e_0 = 0.878) Toyoura sand specimen under cyclic undrained torsional shear (Refer to Figures 6(a) and 6(b) for states A and B).

Director, Institute of Industrial Science. Any opinions, findings, conclusions, or recommendations expressed herein are those of the authors and do not necessarily reflect the views of these funding/supporting organizations.

References

Ampadu, S.I.K., 1991. Undrained behavior of kaolin in torsional simple shear. Ph.D. Thesis, Department of Civil Engineering, University of Tokyo, Japan.

Been, K., Jefferies, M., 2004. Stress dilatancy in very loose sand. Can. Geotech. J. 41 (5), 972–989.

Casagrande, A., 1965. Role of the calculated risk in earthwork and foundation engineering. J. Soil Mech. Found. Division 91 (4), 1–40.

Chiaro, G., 2020. Cyclic resistance and large deformation characteristics of sands under sloping ground conditions: insights from large-strain torsional simple shear tests. Proc. of 7th International Conference on Recent Advances in Geotechnical Earthquake Engineering and Soil Dynamics, State-of-the-Art-and-Practice Lecture paper. 12-15 July 2021, Bangalore, India. Springer, p. 30 (in press).

Chiaro, G., De Silva, L.I.N., Koseki, J., 2017. Modeling the effects of static shear on the undrained cyclic torsional simple shear behavior of liquefiable sand. Geotech. Eng. J. 48 (4), 1–9.

Chiaro, G., Kiyota, T., Koseki, J., 2013a. Strain localization characteristics of loose saturated Toyoura sand in undrained cyclic torsional shear tests with initial static shear. Soils Found. 53 (1), 23–34.

Chiaro, G., Koseki, J., De Silva, L.I.N., 2013b. A density- and stress-dependent elasto-plastic model for sands subjected to monotonic torsional shear loading. Geotech. Eng. J. 44 (2), 18–26.

Chiaro, G., Koseki, J., Sato, T., 2012. Effects of initial static shear on liquefaction and large deformation properties of loose saturated Toyoura sand in undrained cyclic torsional shear tests. Soils Found. 52 (3), 498–510.

Chiaro, G., Umar, M., Kiyota, T., Koseki, J., 2021. Deformation and cyclic strength characteristics of sand under sloping ground conditions: insights from cyclic undrained torsional shear tests with static shear. Geotech. Eng. J. 52 (1), 10, in press.

Hyodo, M., Murata, H., Yasufuku, N., Fujii, T., 1991. Undrained cyclic shear strength and residual shear strain of saturated sand by cyclic triaxial tests. Soils Found. 31 (3), 60–76.

Ishihara, K., Tatsuoka, F., Yasuda, S., 1975. Undrained deformation and liquefaction of sand under cyclic stresses. Soils Found. 15 (1), 29–44.

Kiyota, T., Sato, T., Koseki, J., Abadimarand, M., 2008. Behavior of liquefied sands under extremely large strain levels in cyclic torsional shear tests. Soils Found. 48 (5), 727–739.

Lee, K.L., Albaisa, A., 1974. Earthquake induced settlements in saturated sand. J. Geotech. Eng. Divis. 100 (GT4), 387–406.

Lee, K.L., Seed, H.B., 1967. Dynamic strength of anisotropically consolidated sand. J. Soil Mech. Found. Division ASCE 93 (SM5), 169–190.

Murthy, T.G., Loukidis, D., Carraro, J.A.H., Prezzi, M., Salgado, R., 2007. Undrained monotonic response of clean and silty sands. Géotechnique 57 (3), 273–288.

Robertson, P.K., Fear, C.E., 1995. Liquefaction of sands and its evaluation. Keynote lecture. In: Ishihara, K., Balkema, A.A. (Eds.), Proceedings of the 1st International Conference on Earthquake Geotechnical Engineering, IS Tokyo, Japan, 1253–87.

Seed, H.B., 1983. Earthquake-resistant design of earth dams. Proceedings of the Symposium on Seismic Design Earth Dams and Caverns, New York, pp. 41–46.

Seed, H.B., 1981. Earthquake-resistant design of earth dams. Proceedings of the Symposium on Seismic Design of Earth Dams and Caverns ASCE New York, pp. 41–64.

Seed, H.B., Lee, K.L., Idriss, I.M., Makdisi, F.I., 1975. The slides in the San Fernando dams during the earthquake of February 9, 1971. J. Geotech. Geoenviron. Eng. ASCE 101 (GT7), 651–688.

Sivathayalan, S., Ha, D., 2011. Effect of static shear stress on the cyclic resistance of sands in simple shear loading. Can. Geotech. J. 48 (10), 1471–1484.

Sivathayalan, S., Vaid, Y.P., 2002. Influence of generalized initial state and principal stress rotation on the undrained response of sands. Can. Geotech. J. 39 (1), 63–76.

Tatsuoka, F., Muramatsu, M., Sasaki, T., 1982. Cyclic undrained stress–strain behavior of dense sand by torsional simple shear test. Soils Found. 22 (2), 55–69.

Umar, M., Chiaro, G., Kiyota, T., 2016a. On the influence of initial static shear on large deformation behavior of very loose Toyoura sand in undrained cyclic torsional shear tests. Japanese Geotech. Soc. Special Publ. 4 (2), 17–22.

Umar, M., Chiaro, G., Kiyota, T., 2016b. Effect of initial static shear on strain localization characteristic of loose sand in undrained cyclic torsional shear test. JAEE Annual Meeting, Kochi, Japan, p. 6.

Umar, M., Chiaro, G., Kiyota, T., 2017. Influence of density on large deformation characteristic of sand in undrained cyclic torsional shear tests with initial static shear. Proc. of the 3rd International Conference on Performance-based Design in Earthquake Geotechnical Engineering, Vancouver, Canada, p. 8.

Umar, M., Kiyota, T., Chiaro, G., 2018. Effect of specimen size on behavior of dense sand in large strain torsional shear apparatus. Bull. Earthq. Struct. Res. Center 51, 1–10.

Umar, M., Kiyota, T., Chiaro, G., 2019. Undrained monotonic behavior of sand in large strain torsional shear apparatus. Bull. Earthq. Resistant Struct. Res. Center, Institute of Industrial Science, University of Tokyo 52, 1–10.

Vaid, Y.P., Stedman, J.D., Sivathayalan, S., 2001. Confining stress and static shear effects in cyclic liquefaction. Can. Geotech. J. 38 (3), 580–591.

Vaid, Y.P., Chern, J.C., 1983. Mechanism of deformation during cyclic undrained loading of saturated sands. Int. J. Soil Dyn. Earthquake Eng. 2 (3), 171–177.

Vaid, Y.P., Chern, J.C., 1985. Cyclic and monotonic undrained response of saturated sands. Advances in the Art of Testing Soils under Cyclic Conditions, ASCE Convention, Detroit, USA, pp. 120–147.

Vaid, Y.P., Finn, W.D.L., 1979. Static shear and liquefaction potential. J. Geotechn. Eng. Division, ASCE 105 (GT10), 1233–1246.

Verdugo, R., Ishihara, K., 1996. The steady state of sandy soils. Soils Found. 36 (2), 81–91.

Yang, J., 2002. Non-uniqueness of flow liquefaction line for loose sand. Geotechnique 52 (10), 757–760.

Yang, Z.X., Pan, K., 2017. Flow deformation and cyclic resistance of saturated loose sand considering initial static shear effect. Soil Dyn. Earthquake Eng. 92, 68–78.

Yang, J., Sze, H.Y., 2011. Cyclic behaviour and resistance of saturated sand under non-symmetrical loading conditions. Geotechnique 61 (1), 59–73.

Yoshimi, Y., Oh-oka, H., 1975. Influence of degree of shear stress reversal on the liquefaction potential of saturated sand. Soils Found. 15 (3), 27–40.

Yoshimine, M., Ishihara, K., 1998. Flow potential of sand during liquefaction. Soils Found. 38 (3), 189–198.